Petroleum Science 20 (2023) 857–865

Contents lists available at ScienceDirect

Petroleum Science

journal homepage: www.keaipublishing.com/en/journals/petroleum-science

Original Paper

3D trajectory inversion of an adjacent well using scattered P-wave

Lu Cheng [a, b], Xiao-Hua Che [a, b, *], Wen-Xiao Qiao [a, b], Teng Zhao [a, b]

[a] State Key Laboratory of Petroleum Resources and Prospecting, China University of Petroleum, Beijing, 102249, China
[b] Key Laboratory of Earth Prospecting and Information Technology, Beijing, 102249, China

ARTICLE INFO

Article history:
Received 5 July 2022
Received in revised form
21 October 2022
Accepted 21 February 2023
Available online 22 February 2023

Edited by Jie Hao

Keywords:
Acoustic imaging
Acoustic reflection logging
Directional reception
Adjacent well

ABSTRACT

In oil and gas exploitation, cluster well technology can significantly reduce costs and improve efficiency. An effective adjacent well detection method can greatly reduce the risk of collision between adjacent wells. This study proposes a method to invert the 3D trajectory of an adjacent well using a scattered P-wave obtained by borehole azimuthal acoustic reflection imaging. After obtaining the scattered P-wave from the raw data of the target well using the wave field separation technology, the waveform data in an imaging profile can be obtained by the downhole acoustic directional reception technology. Migration imaging technology is then used to obtain the image of the formation in the imaging profile. Subsequently, by analyzing the images of the formation in the imaging profile of the different azimuths, the well spacing and azimuth of the target well can be determined. Finally, the 3D trajectory of the target well can be obtained by solving the inversion equation. This method was validated by processing the field data from a deviated well in a deep formation. The comparison of the inversion and actual trajectories of the target well demonstrated that the maximum deviation of the inversion trajectory is 0.9 m in the north-south direction, 0.78 m in the east-west direction, 1.45 m in the well spacing, and 2.48° in the azimuth. The field data inversion result demonstrated that the method can effectively use the azimuth reflection acoustic data to invert the 3D trajectory of an adjacent well, which indicates that the borehole azimuthal acoustic reflection imaging technology has great potential within the context of adjacent well detection.

1. Introduction

Cluster well technology is widely used in the development of onshore and offshore oil and gas fields because of its high-efficient and energy-saving; however, adjacent well collision accidents easily occur during drilling (Diao and Gao, 2012; Zhang, 2014; Hong et al., 2020). Anti-collision technology is key in cluster well technology, and effective adjacent well spacing measurement methods can greatly reduce the risk of adjacent well collision. The common method of adjacent well spacing measurement is magnetic ranging, including passive and active magnetic ranging. Although the passive magnetic ranging method does not affect the normal production of the target well, it is heavily dependent on the casing parameters of the target well, and the detection accuracy is also lower. The active magnetic ranging method has higher accuracy but relies on access to the target well with a sensor or emitter, which will affect the normal production of the target well (Zhang et al., 2014; Li et al., 2016; Dou et al., 2018; Dou, 2019). Although certain magnetic ranging methods can be run while drilling, they may be ineffective if formation-linked magnetic anomalies are encountered or the target well is an open hole; however, acoustic methods do not have this limitation because they rely solely on the impedance contrast between the formation and target hole (Gao et al., 2013; Wu et al., 2015; Jervis et al., 2018; Zhang et al., 2020).

By exciting acoustic pulse signals in an exploration well and receiving the echo signals from a geological structure outside the exploration well, borehole acoustic reflection imaging can survey geologic structures (e.g., formation interfaces, caves, and fractures) within a few tens of meters in the formation around the exploration well (Tang and Wei, 2012; Yang et al., 2019a, 2019b; Xu and Hu, 2020; Ben et al., 2021; Li et al., 2021). Because a monopole

Abbreviations: APAR: arcuate phased array receiver, LPAR: linear phased array receiver.

* Corresponding author. State Key Laboratory of Petroleum Resources and Prospecting, China University of Petroleum, Beijing, 102249, China.
E-mail addresses: cldyx1941@foxmail.com (L. Cheng), aclab@cup.edu.cn (X.-H. Che), qiaowx@cup.edu.cn (W.-X. Qiao), zhaotengchn@foxmail.com (T. Zhao).

https://doi.org/10.1016/j.petsci.2023.02.024

source-receiver system is used, monopole P-wave reflection imaging cannot determine the azimuth of the target well; therefore, it is not suitable for adjacent well detection. In contrast, the images of the formation in the imaging profile of different azimuths can be obtained by single-well shear-wave imaging; however, the azimuth determination of the target well has an ambiguity of 180° (Su et al., 2014; Tang et al., 2016a, 2016b, 2021; Lee et al., 2019a, 2019b; Xu et al., 2019; Li et al., 2020; Gu et al., 2021). Because the receiver system is composed of 10 acoustic receiving stations with equal spacing and every acoustic receiving station comprises eight independent sensors, borehole azimuthal acoustic reflection imaging can simultaneously and independently record multichannel acoustic signals (Che et al., 2014, 2016, 2017; Cai, 2016; Ben et al., 2020a; Cheng et al., 2022). Because borehole azimuthal acoustic reflection imaging can not only provide the images of the formation in the imaging profile of different azimuths, but also accurately determine the azimuth of the target well, it has potential for application in adjacent well detection. Ben et al. (2020b) conducted adjacent well detection experiments of borehole azimuthal acoustic reflection imaging, imaged a target well 10.0 m away from the exploratory well, and obtained the azimuth of the target well accurately, but did not provide the 3D trajectory of the target well.

At present, in the case of borehole acoustic reflection imaging in the adjacent well detection, the exploration wells are mostly vertical, and the research on 3D trajectory inversion of target wells is minimal. In this study, a 3D trajectory inversion method for an adjacent well is proposed and owing to the deviation of the exploration well is considered, the method is applicable to both vertical and deviated exploration wells.

2. Methods

2.1. Detecting an adjacent well from the exploration well

Fig. 1 illustrates the configuration for detecting an adjacent well from the exploration well. In Fig. 1, α and β represent the deviation and the deviation azimuth of the exploration well, respectively, and θ represents the azimuth of the imaging profile. The logging instrument is centered in the exploratory well. The receiving acoustic sonde is composed of 10 acoustic receiving stations with equal spacing, and every acoustic receiving station contains eight independent sensors. The source is composed of several monopole transducers with equal spacing. Acoustic pulse signals excited in the exploratory well are obliquely incident to an adjacent well, and the echo signals are received by the receiving acoustic sonde. The clearest images of the adjacent well can be obtained when the imaging profile coincides with the sagittal plane. Additionally, it is worth noting that θ is the azimuth of the adjacent well. Therefore, by analyzing images of the formation in the imaging profile of different azimuths, the well spacing and azimuth of the target well can be obtained.

2.2. Downhole acoustic directional reception

R_i and R_iE_j represent the i-th acoustic receiving station in the receiving acoustic sonde and the j-th sensor in the acoustic receiving station, respectively. In addition, R_iE_1 faces due north when the tool is not rotating. In practical applications, when the space between an adjacent and exploratory well is significantly larger than the size of the receiver array, the event signals from the adjacent well can be regarded as a series of plane waves. As shown in Fig. 2, the incident elevation angle (φ) represents the angle between the incident direction line of the plane wave and the plane of the acoustic receiving station, and the incident azimuth angle (θ') represents the angle between the incident direction line of the plane wave and the sensor (R_iE_1). For simplicity, downhole acoustic directional reception can be decomposed into horizontal plane directional reception and vertical plane scanning reception.

2.2.1. Horizontal plane directional reception

As shown in Fig. 3, point O is the geometric center of acoustic receiving station R_i, and the sensor (R_iE_1) is located due north. Referring to the azimuth angle (θ) of the imaging profile, three adjacent sensors facing the incident direction of the plane-wave are selected from acoustic receiving station R_i to form an arcuate phased array receiver (APAR). For example, a directional receiving waveform in the horizontal plane can be obtained as follows (Ben

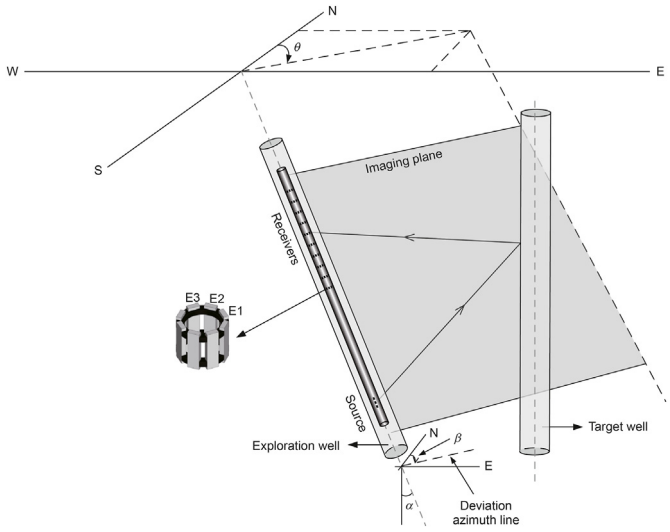

Fig. 1. Configuration for detecting an adjacent well using borehole azimuthal acoustic reflection imaging.

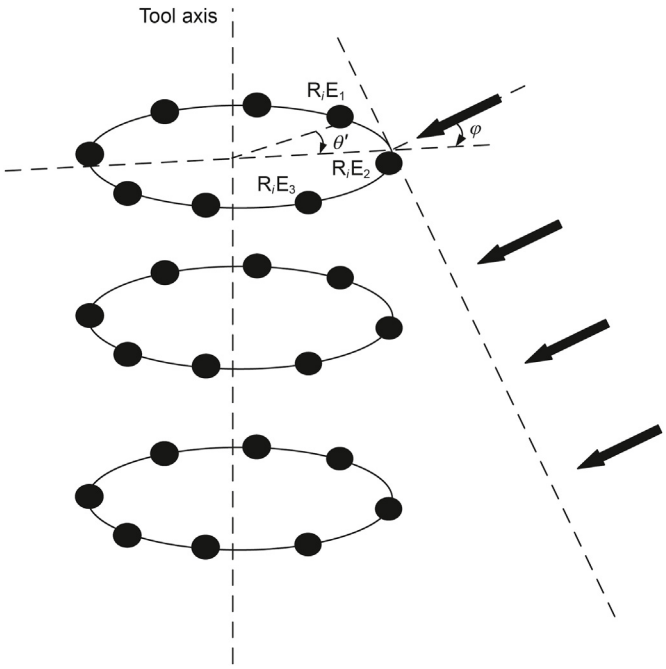

Fig. 2. A plane wave is obliquely incident on the receiving acoustic sonde. Here, θ' is the incident azimuth and φ is the incident elevation.

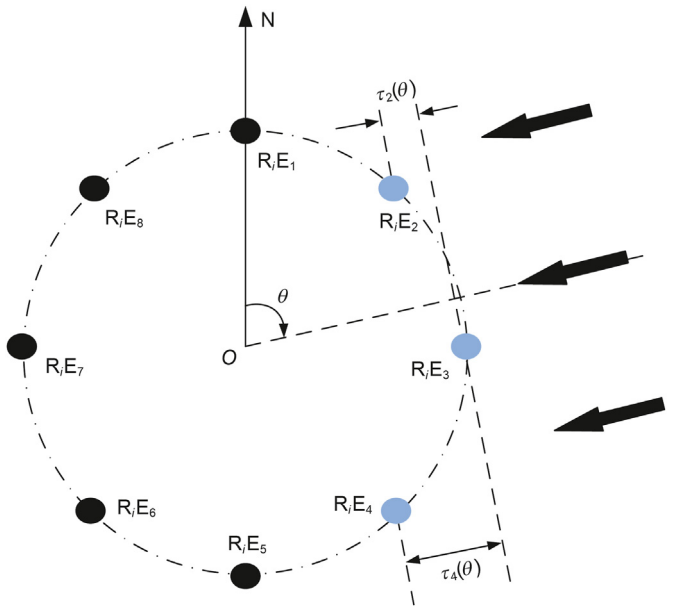

Fig. 3. Delay time calculation for the APAR. Here, θ represents the azimuth of the imaging profile.

et al., 2020a, 2020b):

$$WF_i(\theta,t) = WF_{R_iE_2}(t+\tau_2(\theta)) + WF_{R_iE_3}(t) + WF_{R_iE_4}(t+\tau_4(\theta)) \tag{1}$$

In Eq. (1), $\tau_2(\theta)$ and $\tau_4(\theta)$ represent the delay time of the plane-wave propagation from sensors R_iE_3 to sensors R_iE_2 and R_iE_4, respectively.

2.2.2. Vertical plane scanning reception

As shown in Fig. 4, the sensors on the same azimuth are selected from the adjacent three acoustic receiving stations to form a linear phased array receiver (LPAR). $R_l(l=2,\cdots,9)$ represents the acoustic receiving station where the central sensor of the LPAR is located. The scanning receiving waveform in the vertical plane can be obtained as follows:

$$WF_l(\theta,\varphi',t) = \frac{1}{N}\sum_{i=l-1}^{l+1} WF_i(\theta, t+(l-i)\Delta\tau) \tag{2}$$

In Eq. (2), N represents the number of sensors of LPAR; $\Delta\tau$ represents the delay time of adjacent sensors in LPAR, which can be calculated by the following equation:

$$\Delta\tau = \mathrm{RRSP}\sin(\varphi')/v \tag{3}$$

In Eq. (3), RRSP represents the space between adjacent acoustic receiving stations; v represents the velocity of the plane-wave; and φ' is the scanning reception elevation.

When the scanning reception elevation coincides with the incident elevation, the phase of each waveform used for stacking is identical, and the energy of the scanning receiving waveform is the strongest. For other scanning reception elevations, the energy of the scanning receiving waveform is not significantly enhanced or even weakened. Therefore, comparing the energy of the scanning reception waveforms with different scanning reception elevations, the waveform with the strongest energy is the directional reception waveform in the imaging profile.

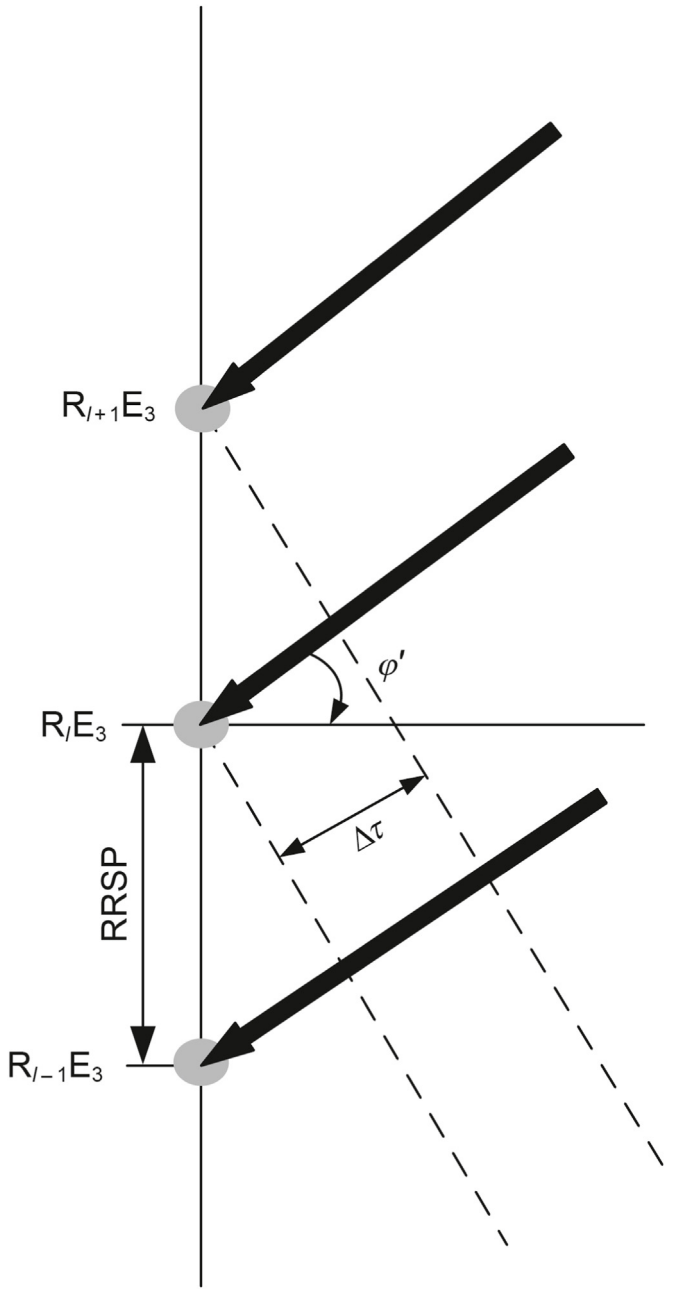

Fig. 4. Delay time calculation for the LPAR. Here, φ' represents the scanning reception elevation.

2.3. 3D trajectory inversion method for an adjacent well

Fig. 5 is the schematic diagram of the 3D trajectory inversion of an adjacent well. Point M represents a point on the adjacent well in the image and line segment MB is perpendicular to the axis of the exploratory well. α_B and β_B respectively represent the deviation and the deviation azimuth of point B on the exploration well, and θ_M is the azimuth of the imaging profile. As shown in Fig. 5, the reference coordinate system (xyz) and global coordinate system ($x'y'z'$) were established with point B as the origin. The z-axis coincides with the axis of the exploration well, the z'-axis coincides with the gravity line, and the projection of the x-axis and x'-axis positive directions are both northwards.

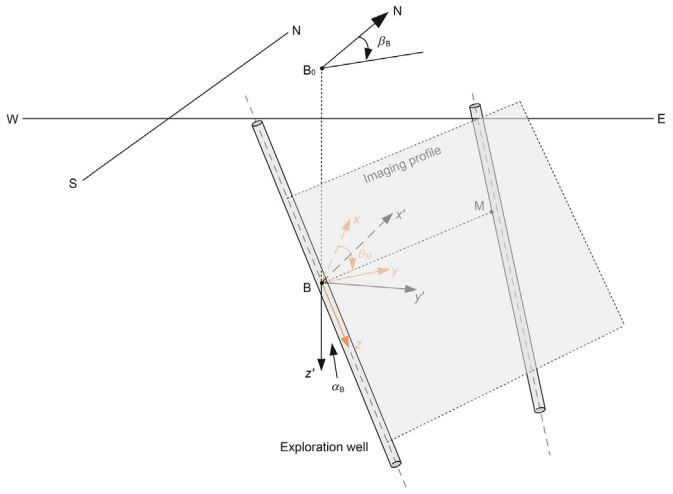

Fig. 5. Schematic of the 3D trajectory inversion.

The global coordinate system $(x'y'z')$ can be obtained by rotating the reference coordinate system (xyz). The detailed steps are as follows: first, a temporary coordinate system $(x_1y_1z_1)$ can be obtained through clockwise rotation of the reference coordinate system (xyz), where the x-axis is the rotation axis and β_B is the rotation angle; Then, the global coordinate system $(x'y'z')$ can be obtained through clockwise rotation of the coordinate system

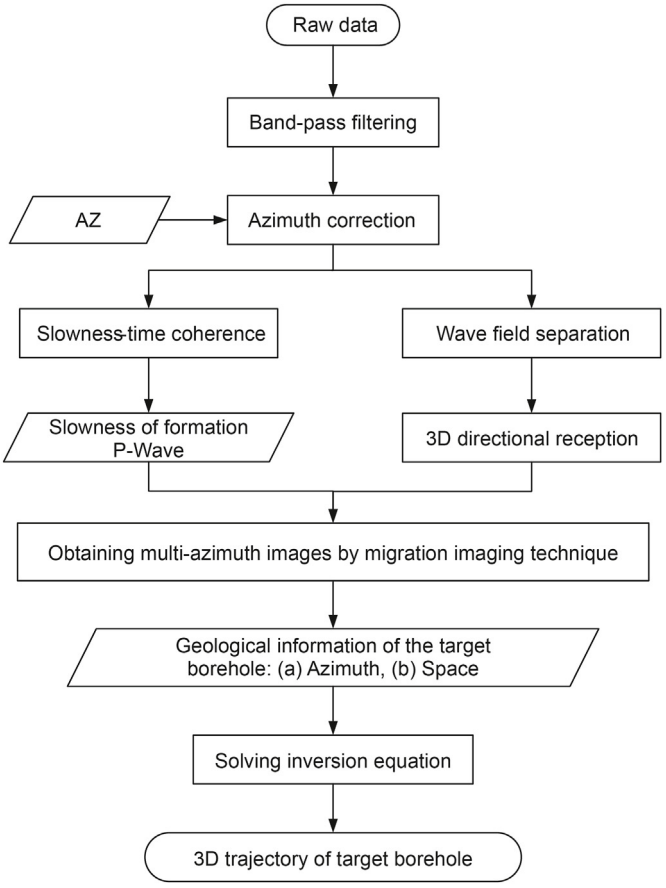

Fig. 6. Processing workflow for field data.

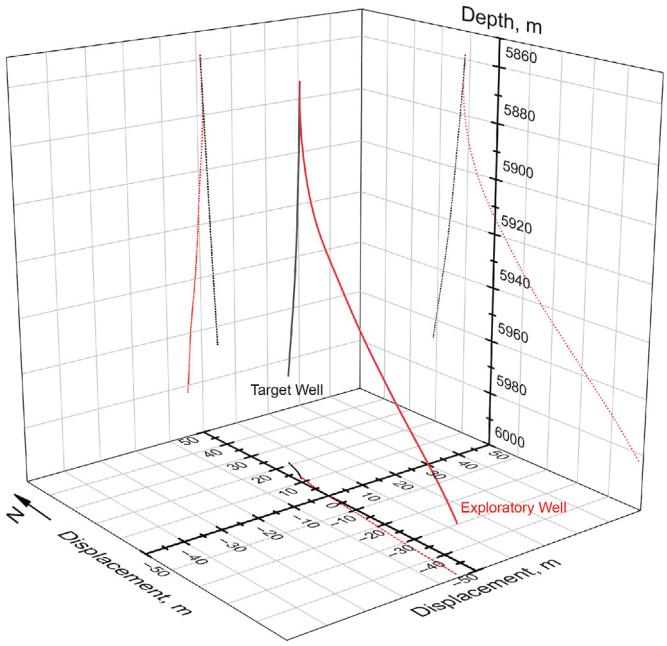

Fig. 7. Schematic of the two adjacent wells.

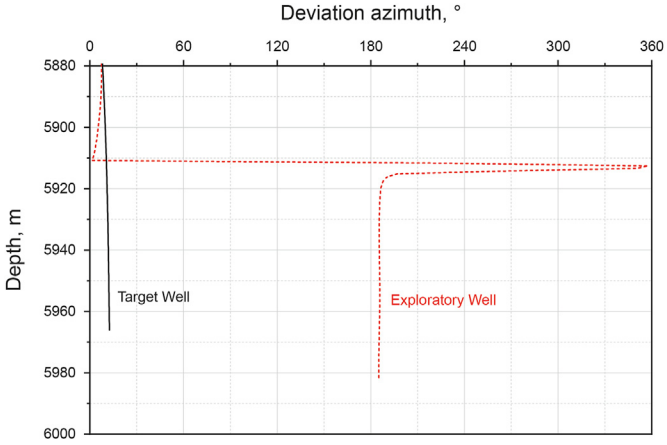

Fig. 8. Deviation azimuths of the two wells.

$(x_1y_1z_1)$, where the y_1-axis is the rotation axis and α_B is the rotation angle. Based on the right-hand coordinate system, the counterclockwise rotation is positive, and the above rotation can be expressed as (Zhang et al., 2021):

$$\begin{bmatrix} x'_M \\ y'_M \\ z'_M \end{bmatrix} = \mathbf{R}_y(\alpha_B)\mathbf{R}_x(\beta_B) \begin{bmatrix} x_M \\ y_M \\ z_M \end{bmatrix} \tag{4}$$

In Eq. (4), $\boldsymbol{R}_x$ and $\boldsymbol{R}_y$ are rotation matrices, which are expressed as:

$$\mathbf{R}_x(\beta_B) = \begin{bmatrix} 1 & 0 & 0 \\ 0 & \cos\beta_B & \sin\beta_B \\ 0 & -\sin\beta_B & \cos\beta_B \end{bmatrix}, \mathbf{R}_y(\alpha_B) = \begin{bmatrix} \cos\alpha_B & 0 & -\sin\alpha_B \\ 0 & 1 & 0 \\ \sin\alpha_B & 0 & \cos\alpha_B \end{bmatrix} \tag{5}$$

In the reference coordinate system (xyz), based on the geometric relationship, the following can be obtained:

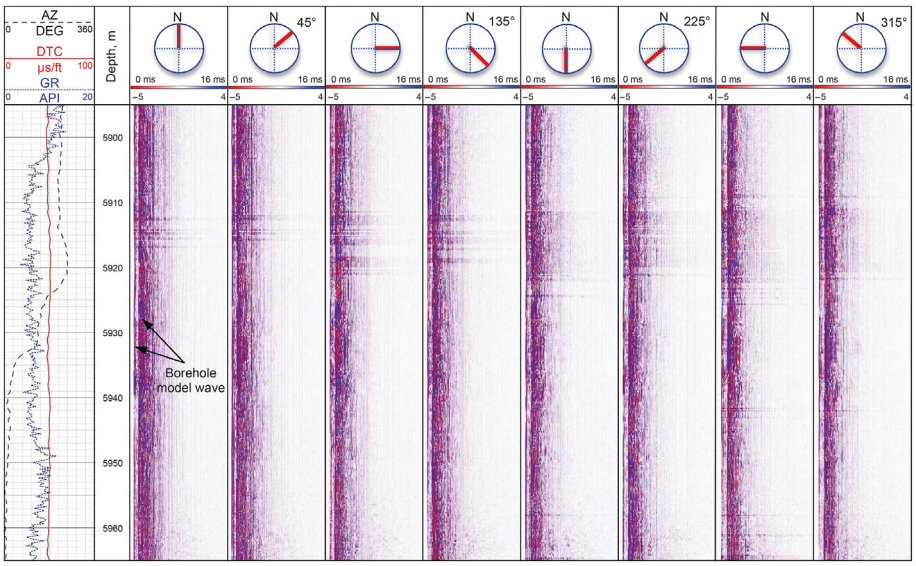

Fig. 9. Raw waveforms recorded by the acoustic receiver station R_1.

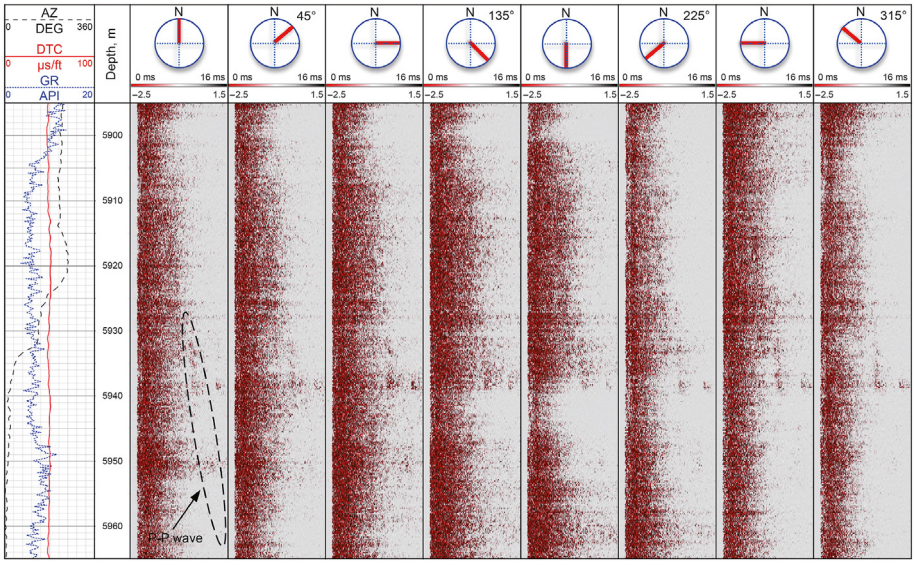

Fig. 10. Scattered P–P wave from the target well recorded by the acoustic receiver station R_1.

$$\begin{cases} x_M = \overline{BM}\cos\theta_M \\ y_M = \overline{BM}\sin\theta_M \end{cases} \quad (6)$$

In Eq. (6), θ_M is the azimuth of the imaging profile.

2.4. Processing workflow for field data

The workflow for the 3D trajectory inversion of an adjacent well using field data is shown in Fig. 6. First, the low- and high-frequency noises in the raw data were removed by band-pass filtering, and azimuth correction was implemented in combination with the AZ curve. Subsequently, the slowness-time coherence method was used to obtain the slowness of the formation P-wave, and the event signals from the adjacent well were extracted by using *f-k* filtering. The waveform data in an imaging profile can be obtained by using downhole acoustic directional reception technology. Migration imaging methods were then used to obtain the image of the formation in the imaging profile. (Lee et al., 2019a, 2019b; Ben et al., 2020b; David et al., 2020; Huo et al., 2020). Then, by analyzing the images of the formation in the imaging profile of different azimuths, the well spacing and azimuth of the target well can be determined. Finally, the 3D trajectory of the target well can be determined by solving the inversion equation.

3. Results of field data

First, we introduced the background of the field data. The 3D trajectories of two wells are shown in Fig. 7, in which the exploratory well is deviated and the target well is vertical. The target well is an oil production well located in an anticline structure with a borehole diameter of 0.2 m, and below 5840 m, it is an open hole. The exploratory well is a sidetracked well of the target well. Fig. 8

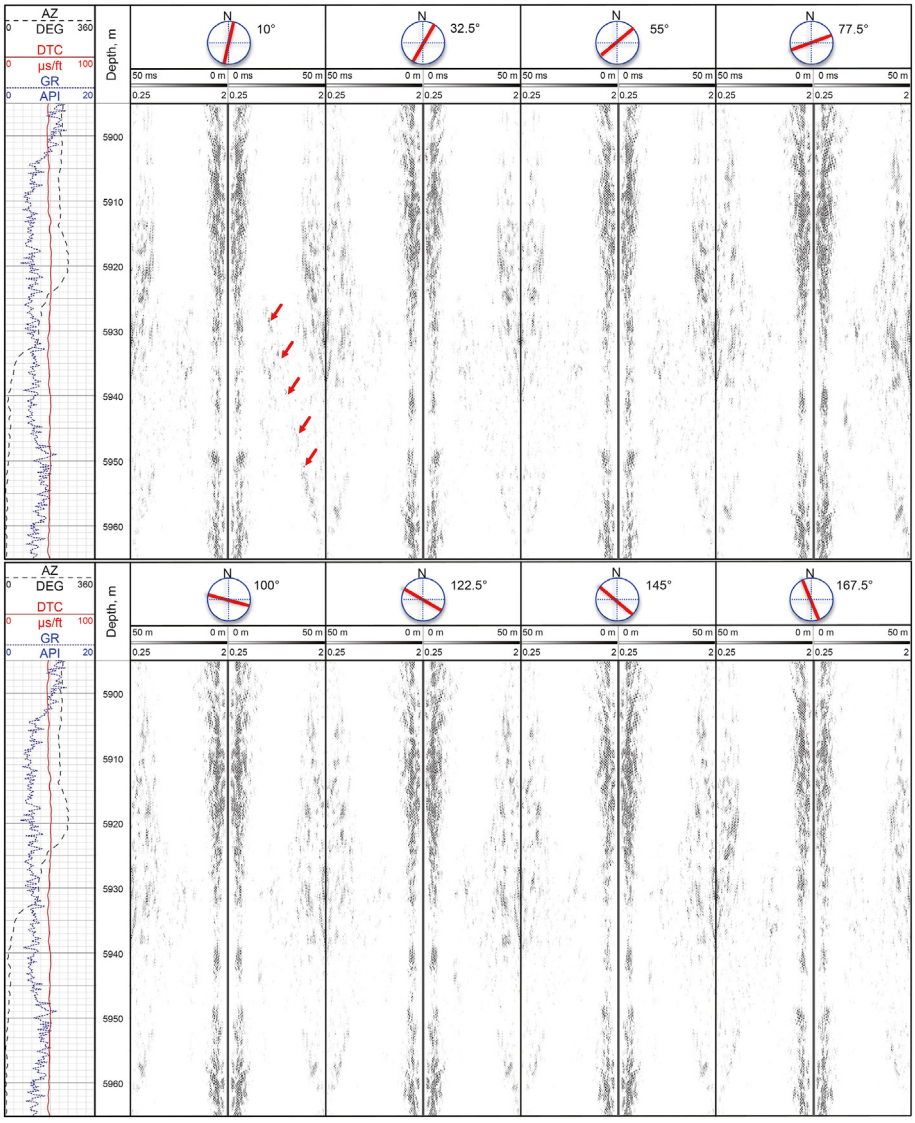

Fig. 11. Migration images for the scattered P–P wave at 16 azimuths.

shows the deviation azimuth of exploration well and target well at 5880–6000 m depth. Below 5920 m, the deviation azimuths of two wells are constant.

3.1. Scattered P-wave extraction

Fig. 9 shows the recorded raw waveforms of the acoustic receiver station R_1. The AZ curve records the rotation of the tool during the working process; the DTC curve is the formation compressional wave slowness obtained via the slowness-time coherence method; the GR curve is the total gamma-ray value of the formation. The characteristics of the borehole mode waves are evident, the amplitudes are large, but the event signals from the target well cannot be observed. The event signals (marked by a black dotted ellipse) from the target well are extracted from the raw waveforms using band-pass (8–14 kHz) and *f-k* filtering, as shown in Fig. 10. Although the target well is vertical, the exploration well where the tool is located is inclined. Therefore, in Fig. 10, the phase axis of the P–P mode echo from the target well is inclined. The velocity of the compressional wave in the formation is approximately 6096 m/s; the dominant frequency of the source of the logging instrument is approximately 14.0 kHz; thus, the wavelength of the compressional wave in the formation is approximately 0.435 m. Therefore, the P–P mode echo from the target well is a scattered P-wave with a weaker amplitude.

3.2. Migration images

After the waveform data in an imaging profile are acquired using downhole acoustic directional reception technology, migration imaging technology is used to obtain the formation image in the imaging profile. Fig. 11 shows the migration images for the scattered P–P wave, and the first panel is the same as that in Fig. 9. Fig. 11 shows that the imaging characteristics of the scattered P–P wave from the target well are obvious at depths of 5924–5964 m (marked by the red arrow), and the imaging amplitude varies with the azimuth. Owing to the acoustic and electrical isolation between adjacent receiving sensors, the receiving sensors facing the target well can more effectively record the scattered P–P wave from the target well. Therefore, the scattered P–P wave from the target well recorded by the receiving sensor located closer to the azimuth of the target well has a larger amplitude. When the amplitude of the

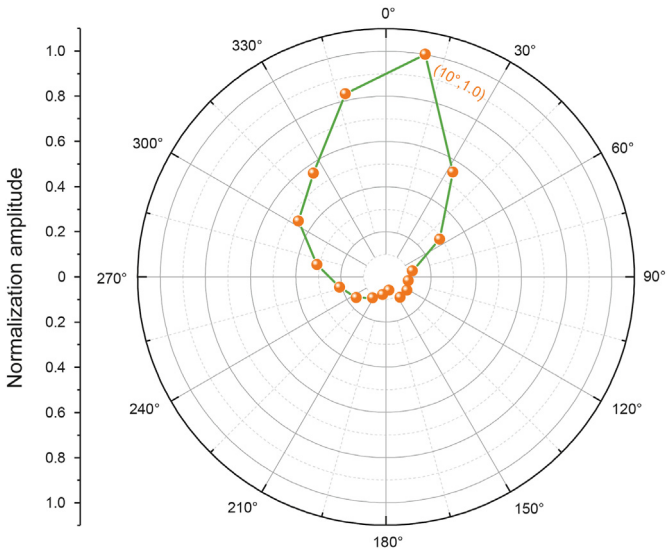

Fig. 12. Normalization imaging amplitude of the target well versus the azimuth of the imaging profile.

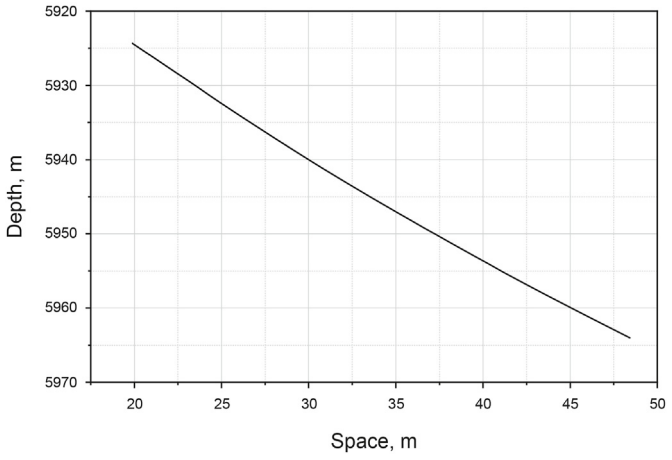

Fig. 13. Space between the exploration and target wells at different depths.

scattered P–P wave is larger, the imaging amplitude in the migration image is as well. Because the deviation azimuth of the target well is almost constant below 5920 m, the sum of the imaging amplitude at each depth can be used to represent the imaging amplitude of the target well. Fig. 12 shows the normalization imaging amplitude of the target well versus the azimuth of the imaging profile; thus, the measured azimuth of the target well is 10°, which is close to the azimuth of the target well. Fig. 13 shows the space between the exploration and target wells at different depths obtained by the migration images.

3.3. 3D trajectory inversion of the target well

After obtaining the well spacing and azimuth of the target well, the 3D trajectory of the target well can be obtained by solving Eq. (4), as shown in Fig. 14. Fig. 14 shows that the 3D trajectory of the target well obtained by using the field-data inversion is in agreement with the actual 3D trajectory. Then, the space and azimuth deviation between the inversion trajectory of the target well and the real trajectory are calculated, as shown in Fig. 15. The comparison of the inversion and actual trajectories of the target well

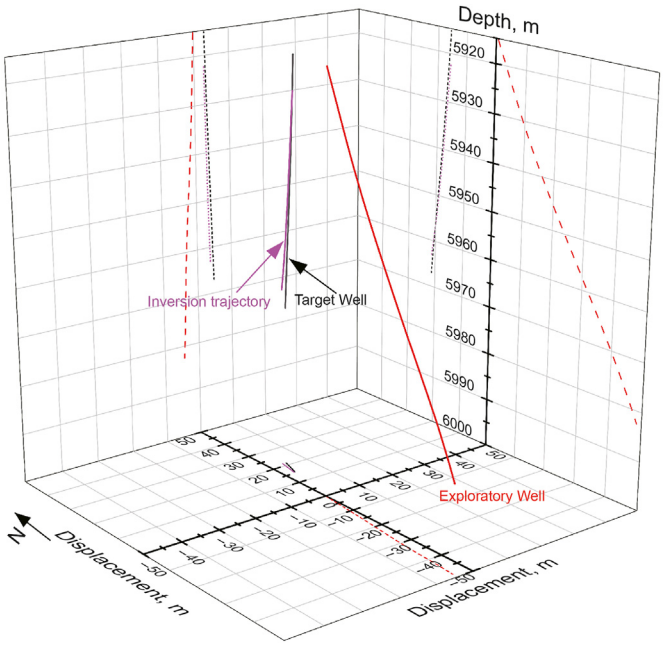

Fig. 14. 3D trajectory inversion results for the target well.

demonstrated that the maximum deviation of the inversion trajectory is 0.9 m in the north-south direction, 0.78 m in the east-west direction, 1.45 m in the well spacing, and 2.48° in the azimuth.

4. Conclusions

An effective adjacent well detection method can greatly reduce the risk of collision between adjacent wells during cluster well construction. In this study, we proposed a method to invert the 3D trajectory of an adjacent well using the scattered P–P wave obtained by borehole azimuthal acoustic reflection imaging. In this method, the scattered P-wave from the target well is extracted from the raw data by using wavefield separation technology. Then, referring to the azimuth of an imaging profile, the directional receiving waveform in the horizontal plane can be obtained using horizontal plane directional reception method, and the scanning reception waveforms with different scanning reception elevations in the vertical plane can be obtained using vertical plane scanning reception method. Comparing the energy of the scanning reception waveforms with different scanning reception elevations, the waveform with the strongest energy is the directional reception waveform in the imaging profile. Migration imaging technology can be used to obtain the formation image in the imaging profile. Subsequently, by analyzing the images of the formation in the imaging profile of different azimuths, the well spacing and azimuth of the target well can be determined. Finally, the 3D trajectory of the target well can be obtained by solving the inversion equation.

To verify the method, it was used to process the field data from an inclined well in a deep formation. The comparison of the inversion and actual trajectories of the target well demonstrated that the maximum deviation of the inversion trajectory is 0.9 m in the north-south direction, 0.78 m in the east-west direction, 1.45 m in the well spacing, and 2.48° in the azimuth. The field data inversion result demonstrated that the method can effectively use the scattered P–P wave to invert the 3D trajectory of the adjacent well, suggesting that borehole azimuthal acoustic reflection imaging technology has great potential for adjacent well detection. However, borehole azimuthal acoustic reflection imaging

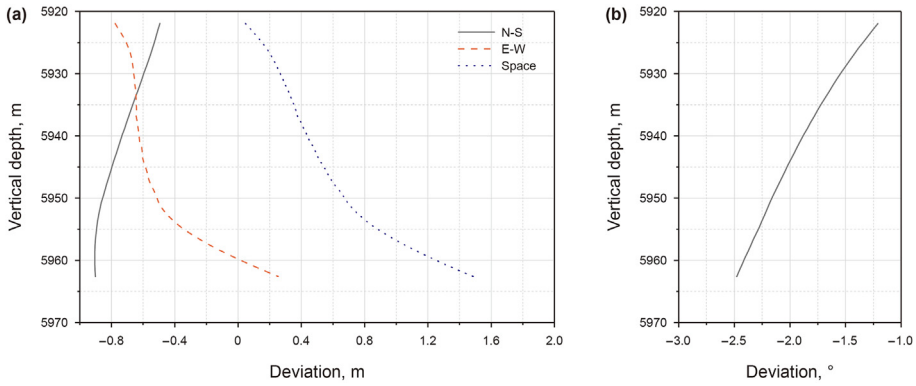

Fig. 15. Deviation analysis of inversion results: (a) displacement and (b) azimuth deviations.

technology has some limitations; specifically, it has a long data processing time and cannot run while drilling. Our future work will address these limitations.

Acknowledgements

This work is supported by the National Natural Science Foundation of China (grant numbers 12274465, 42174218) and the Strategic Cooperation Technology Projects of CNPC and CUPB (grant number ZLZX2020-02).

Data availability

The processed data required to reproduce these findings cannot be shared at this time as the data also form a part of an ongoing study.

Declaration of competing interest

The authors declare that they have no known competing financial interests or personal relationships that could have appeared to influence the work reported in this paper.

References

Ben, J.L., Qiao, W.X., Che, X.H., et al., 2020a. Experimental simulation of obtaining the reflector azimuth using azimuthal acoustic reflection tool in the underwater environment. J. Pet. Sci. Eng. 195, 107649.

Ben, J.L., Qiao, W.X., Che, X.H., et al., 2020b. Field validation of imaging an adjacent borehole using scattered P-waves. Petrol. Sci. 17 (5), 1272–1280.

Ben, J.L., Che, X.H., Qiao, W.X., et al., 2021. Application of near-borehole geologic reflector evaluation using azimuthal acoustic reflection imaging logging. Well Logging Technol. 45 (1), 23–29 (in Chinese). https://doi.org/10.16489/j.issn.1004-1338.2021.01.004

Cai, M., 2016. Study on Signal Processing Method for Borehole Azimuthal Acoustic Reflection Imaging Logging. Ph.D. thesis. Beijing: China University of Petroleum, Beijing (in Chinese).

Cheng, L., Qiao, W.X., Che, X.H., Zhao, T., 2022. A 3-D plane-wave beamforming method for borehole azimuthal acoustic reflection imaging. Geophys. J. Int. 230 (3), 1652–1661. https://doi.org/10.1093/gji/ggac149

Che, X.H., Qiao, W.X., Ju, X.D., et al., 2014. An experimental study on azimuthal reception characteristics of acoustic well-logging transducers based on phased-arc arrays. Geophysics 79 (3), D197–D204. https://doi.org/10.1190/GEO2013-0334.1

Che, X.H., Qiao, W.X., Ju, X.D., et al., 2016. Experimental study of the azimuthal performance of 3D acoustic transmitter stations. Petrol. Sci. 13 (1), 52–63. https://doi.org/10.1007/s12182-015-0073-2

Che, X.H., Qiao, W.X., Ju, X.D., et al., 2017. Experimental study on the performance of an azimuthal acoustic receiver sonde for a downhole tool. Geophys. Prospect. 65 (1), 158–169. https://doi.org/10.1111/1365-2478.12401

Diao, B.B., Gao, D.L., 2012. Calculation method of adjacent well oriented separation factors. Pet. Drill. Techn. 40 (1), 22–27. https://doi.org/10.3969/j.issn.1001-0890.2012.01.005

Dou, X.Y., Liang, H.Q., Liu, Y., 2018. Anticollision method of active magnetic guidance ranging for cluster wells. Math. Probl Eng. 1–11. https://doi.org/10.1155/2018/7583425

Dou, X.Y., 2019. Research on Magnetic Positioning Method of Adjacent Well Spacing in Cluster Wells. Ph.D. thesis. Beijing: China University of Petroleum, Beijing (in Chinese).

David, L., Tian, X., Tang, X.M., et al., 2020. Gaussian beam imaging of fractures near the wellbore using sonic logging tools after removing dispersive borehole waves. Geophysics 85 (4), D133–D143. https://doi.org/10.1190/GEO2019-0104.1

Gao, D.L., Diao, B.B., Wu, Z.Y., Zhu, Y., 2013. Research into magnetic guidance technology for directional drilling in SAGD horizontal wells. Petrol. Sci. 10 (4), 500–506. https://doi.org/10.1007/s12182-013-0301-6

Gu, X.H., Tang, X.M., Su, Y.D., 2021. Delineating a cased borehole in unconsolidated formations using dipole acoustic data from a nearby well. Geophysics 86 (5), D139–D147. https://doi.org/10.1190/GEO2020.0570.1

Hong, D.F., Tang, X.P., Gao, W.K., et al., 2020. A new calculation approach of wellbore separation factor based on the relative position of adjacent wells. Pet. Expl. Dev. 47 (1), 186–192. https://doi.org/10.1016/S1876-3804(20)60018-0.

Huo, J.J., Zhou, B.Z., Zhao, Q., Mason, I.M., 2020. Reconstruction of borehole radar images by a modified f–k migration. Geophys. J. Int. 221 (3), 1626–1634. https://doi.org/10.1093/gji/ggaa094

Jervis, M., Tonellot, T., Baukulin, A., Ghamdi, I.A., 2018. High-resolution acoustic imaging from a borehole to detect a nearby well. Lead. Edge 37 (11), 812–817. https://doi.org/10.1190/tle37110812.1

Lee, S.Q., Cheng, M., Gu, X.H., et al., 2019a. Application of four-component dipole shear reflection imaging to interpret the geological structure around a deviated well. Appl. Geophys. 16 (3), 291–301.

Lee, S.Q., Tang, X.M., Su, Y.D., 2019b. Shear wave imaging to determine near-borehole faults for ocean drilling exploration. Geophys. J. Int. 217 (1), 288–293.

Li, C., Gao, D.L., Liu, Q.L., Kong, X., 2016. A method of calculating of avoiding collisions with adjacent wells using electromagnetic ranging surveying while drilling tools. Pet. Drill. Tech. 44 (5), 52–59. https://doi.org/10.11911/syztjs.201605009

Li, Y.H., Tang, X.M., Li, H.R., Lee, S.Q., 2020. Characterizing the borehole response for single-well shear-wave reflection imaging. Geophysics 86 (1), D15–D26. https://doi.org/10.1190/GEO2020-0212.1

Li, D., Qiao, W.X., Che, X.H., et al., 2021. Eliminating the azimuth ambiguity in reflected S-wave imaging logging based on the azimuthal receiver mode. J. Pet. Sci. Eng. 199, 108295. https://doi.org/10.1016/j.petrol.2020.108295

Su, Y.D., Wei, Z.T., Tang, X.M., 2014. A validation method of dipole shear-wave remote reflection imaging from adjacent borehole reflection. J. Appl. Acoust. 33 (1), 29–34 (in Chinese). https://doi.org/10.11684/j.issn.1000-310X.2014.01.005

Tang, X.M., Wei, Z.T., 2012. Significant progress of acoustic logging technology: remote acoustic reflection imaging of a dipole acoustic system. J. Appl. Acoust. 31 (1), 10–17 (in Chinese).

Tang, X.M., Cao, J.J., Li, Z., Su, Y., 2016a. Detecting a fluid-filled borehole using elastic waves from a remote borehole. J. Acoust. Soc. Am. 140 (2), EL211–EL217.

Tang, X.M., Li, Z., Hei, C., Su, Y., 2016b. Elastic wave scattering to characterize heterogeneities in the borehole environment. Geophys. J. Int. 205 (1), 594–603.

Tang, X.M., Gu, X.H., Li, Y.H., Su, Y., 2021. The interaction between borehole and elastic waves: theory, method and application. Chin. J. Geophys. 64 (12), 4227–4238 (in Chinese). https://doi.org/10.6038/cjg202100396

Wu, Z.Y., Gao, D.L., Diao, B.B., 2015. An investigation of electromagnetic anti-collision real-time measurement for drilling cluster wells. J. Nat. Gas Sci. Eng. 23, 346–355. https://doi.org/10.1016/j.jngse.2015.02.016

Xu, J.Q., Hu, H.S., Wang, Z., 2019. Asymptotic solution to a 3D dipole single-well imaging system with combined monopole and dipole receivers with an application in elimination of azimuth ambiguity. Geophysics 84 (5), D191–D207. https://doi.org/10.1190/GEO2018-0658.1

Xu, J.Q., Hu, H.S., 2020. Solutions of P-SV and SV-P waves in single-well imaging through reciprocity relations. Geophysics 85 (6), D245–D259. https://doi.org/

10.1190/GEO2019-0551.1
Yang, S.B., Qiao, W.X., Che, X.H., Ju, X., 2019a. Numerical simulation of acoustic reflection logging while drilling based on a cylindrical phased array acoustic receiver station. J. Pet. Sci. Eng. 183, 106467.
Yang, S.B., Qiao, W.X., Che, X.H., 2019b. Numerical simulation of acoustic fields in formation generated by linear phased array acoustic transmitters during logging while drilling. J. Pet. Sci. Eng. 182, 106184.
Zhang, S., 2014. Magnetic Interference Effects on the Magnetic Parameters of Wellbore Survey and Adjacent Wells Ranging Method. Ph.D. Thesis. East. China University of Petroleum (East) (in Chinese).
Zhang, S., Guan, Z.C., Wang, J.Y., Shi, Y., 2014. Detect adjacent well by analyzing geomagnetic anomalies. Res. J. Appl. Sci. Eng. Technol. 7 (11), 2353–2361.
Zhang, S., Diao, B.B., Gao, D.L., 2020. Numerical simulation and sensitivity analysis of accurate ranging of adjacent wells while drilling. J. Pet. Sci. Eng. 195, 107536. https://doi.org/10.1016/j.petrol.2020.107536
Zhang, X.Q., Wen, X.T., Zhang, C.M., et al., 2021. Three-dimensional rotation curvature attribute method based on coordinate transformation. Comput. Tech. Geophys. Geochem. Explor. 43 (5), 543–553 (in Chinese). https://doi.org/10.3969/j.issn.1001-1749.2021.05.02